Li, Yun; Taskinen, Pekka; Wang, Yuejun; Yang, Shenghai; Tang, Chaobo; Chen, Yongming; Jokilaakso, Ari

$PbSO_4$ Reduction Mechanism and Gas Composition at 600–1000°C

Published in:
JOM

DOI:
10.1007/s11837-020-04551-4

Published: 01/03/2021

Document Version
Peer-reviewed accepted author manuscript, also known as Final accepted manuscript or Post-print

Please cite the original version:
Li, Y., Taskinen, P., Wang, Y., Yang, S., Tang, C., Chen, Y., & Jokilaakso, A. (2021). $PbSO_4$ Reduction Mechanism and Gas Composition at 600–1000°C. *JOM*, *73*(3), 881-891. https://doi.org/10.1007/s11837-020-04551-4

$PbSO_4$ reduction mechanism and gas composition at 600-1000 °C

YUN Li [1, 2], PEKKA TASKINEN [3], YUEJUN WANG [4], SHENGHAI YANG [1, 2], CHAOBO TANG [1, 2], YONGMING CHEN [1, 2, 5], and ARI JOKILAAKSO [1, 3]

1.—School of Metallurgy and Environment, Central South University, Changsha, Hunan, 410083, P.R China. 2.—National Engineering Laboratory for High Efficiency Recovery of Refractory Nonferrous Metals, Changsha, Hunan, 410083, P.R China. 3.—Department of Chemical and Metallurgical Engineering, Aalto University, Espoo, 02150, Finland. 4.—Department of Ecology and Resources Engineering, Hetao College, Inner Mongolia Bayannur, 015000, China. 5.—e-mail: csuchenyongming@163.com.

ABSTRACT

A promising lead-containing wastes recycling method, with sulfur conservation and reductive sulfur-fixing co-smelting process (RSFCS), is proposed. This work investigated the $PbSO_4$ reduction equilibrium composition, phase conversions, and microscopic transformation mechanisms during the RSFCS process at different temperatures, times, and CO-CO_2 mixtures using thermodynamic modelling, thermogravimetric analysis, x-ray diffraction, and SEM-EDS analysis techniques. At the same time, the gaseous products were collected and analyzed. The results showed that three reduction paths existed: (1) $PbSO_4 \xrightarrow{CO/CO_2} PbO\cdot PbSO_4 + SO_2 \xrightarrow{CO/CO_2} 2PbO\cdot PbSO_4 + SO_2 \xrightarrow{CO/CO_2} 4PbO\cdot PbSO_4 + SO_2 \xrightarrow{CO/CO_2} PbO + SO_2 \xrightarrow{CO/CO_2} Pb$; (2) $PbSO_4 \xrightarrow{CO/CO_2} PbS$; (3) $PbSO_4 \rightarrow PbO\cdot PbSO_4 + SO_3 \rightarrow 2PbO\cdot PbSO_4 + SO_3 \rightarrow 4PbO\cdot PbSO_4 + SO_3 \rightarrow PbO + SO_3$. Reduction temperature and CO concentration were determined as major factors in the $PbSO_4$ reduction. In a relatively weak reductive atmosphere and at low temperature, $xPbO\cdot PbSO_4$ (x=1, 2, 4), PbO, Pb and SO_2 were the major products. When temperature and the CO concentration increased, $PbSO_4$ was selectively reduced to PbS, with sulfur in $PbSO_4$ fixed in PbS, instead of emitting SO_2/SO_3.

INTRODUCTION

A large amount of lead-containing waste is generated and discharged annually from metallurgical, chemical, electronic and environmental industries worldwide [1], including lead-acid battery paste [2], zinc hydrometallurgical residues (hot acid leaching residues, jarosite and goethite residues etc.), smelting dusts and ashes, electrolytic anode slimes and scrubber sludges, etc. [3, 4]. These kinds of wastes are generally characterized by a wide range of sources, complex properties and variable components [5], that make them very difficult to deal with. For example, lead is present in the forms of $PbSO_4$, PbS, PbO_2, PbO, $PbSiO_3$ and metallic Pb [6], regardless of other components, like zinc (Zn), copper (Cu), antimony (Sb), bismuth (Bi), iron (Fe), gold (Au), silver (Ag) and hazardous cadmium (Cd), arsenic (As), chromium (Cr) and mercury (Hg) [7]. In many countries, these lead-bearing wastes are classified as hazardous waste due to the toxicity of some heavy metals, e.g. lead and/or arsenic [8]. They are greatly detrimental to environment and human health if left untreated or abandoned directly in the environment [9].

Over the last few decades, recycling and harmless disposal are two alternatives for treatment of waste materials [3, 10]. Harmless disposal techniques [11], however, do not recover the metal values in the wastes. Therefore, recycling is the most promising method for the sustainable development of the industry and our society [2]. The recycling technologies consist of pyrometallurgy, hydrometallurgy [12] and electrometallurgy .[13] Pyrometallurgy acts as the dominant method for primary lead production and also the secondary lead recycling [8]. In China, double-side blowing and bottom blowing techniques are two advanced techniques, represented by Anhui Huabo, Narada, (http://www.naradahb.com/). It employs double-side blowing technique to treat 0.6 million tonnes lead-acid paste and around 67 thousand tonnes other lead-containing waste materials per year. Another representative company, Henan Yuguang Gold and Lead, (http://www.yuguanggold-lead.com.cn/), uses bottom blowing to treat 0.4 million tones lead paste annually. Hydrometallurgy processes are usually considered as low cost and green technologies. [2, 14] However, the current hydrometallurgical techniques are less competitive than pyrometallurgy in secondary materials recycling and treatment, because of their laborious procedures, low efficiency and processing capacity, as well as generation of large amounts of problematic waste water and residues [15, 16].

However, current pyrometallurgical technologies are always accompanied with high temperature and high energy consumption, poor operational conditions and emissions [17], especially in the disposal of

secondary lead-bearing wastes. The problems are particularly serious. The sulfur content in the waste materials is lower than the primary lead concentrates. As a result, if a current pyrometallurgical technique were employed to recycle lead-containing wastes, the SO_2 in the smelting off-gas generally fluctuates between 0.05~2 vol%, which is lower than that of primary lead smelting (typically 7~12 vol%)[18]. Thus, it is hard to reach the general sulfuric acid making (SAM) off-gas level (SO_2 vol% > 4 vol%). Alternatively, H_2SO_4-making from low concentration SO_2 tail gas or desulfurization treatment (apply to SO_2 vol% < 1 vol%) is available [19], but the cost is high. At the same time, the SAM using lean 1~4 vol% SO_2 gas has been a technical bottleneck [18]. Therefore, the disposal of flue gas containing low concentration SO_2 formed from lead-containing waste treatment has always been a serious challenge.

The authors proposed a promising cleaner and short-flowsheet technique, named as reductive sulfur-fixing co-smelting process (RSFCS) [20, 21], to recycle and recover various valuable metals from lead-containing waste mixtures [22]. This novel technique is distinguished from the conventional pyrometallurgy techniques by a reducing atmosphere in the processing, combined with sulfur transformation and fixation as a sulfide matte. Thus, the generation and emissions of SO_2/SO_3 are expected to be low [5]. At the same time, the lead components would expect to be rapidly reduced and decomposed to easy-recycled by-products, such as PbO, Pb and PbS [16].

$PbSO_4$, as one of the dominant and refractory components in lead-containing wastes [23, 24], has a reduction behavior that not only affects lead recovery but also determines the generation and emissions of sulfur-containing gases. Studies were devoted to dissociation of metal sulfates [25, 26], but less attention has been paid to $PbSO_4$ reduction. This study investigated the $PbSO_4$ reduction mechanism at different temperatures, reduction times and atmospheres. MTDATA ver. 8.2 [27] software and its MTOX database [28] were firstly used to model thermodynamically the gas-liquid-solid phases equilibrium compositions at different temperatures during the $PbSO_4$ decomposition and reduction process. Furthermore, thermogravimetric analysis, XRD and SEM-EDS techniques were employed to investigate the $PbSO_4$ reduction behavior, phase conversion and microscale transformation mechanisms. Moreover, the gaseous products generated at different temperatures, times and CO-CO_2 mixtures were collected and analyzed for inferring the formation mechanisms of the sulfur-bearing off-gas.

EXPERIMENTAL MATERIALS AND METHODS

High purity $PbSO_4$ powder (99.99 % purity, Aladdin Industrial Corporation, China) was used to ensure a high experimental accuracy. $PbSO_4$ powder was dried at 85 °C for 24 h to remove moisture and crystal water. The dry $PbSO_4$ powder was prepared for thermogravimetric analysis (STA 494 F3; NETZSCH, Germany) and isothermal reduction experiments. CO and CO_2 (99.99 % purity) were used to provide different CO-CO_2 concentrate mixture. The experimental $PbSO_4$ reduction study was carried out in a horizontal tube furnace equipped with a gas and temperature controller (SR3-8P-N-90-100Z, SHIMADEN Co., Ltd., Japan, accuracy ±1 °C), as shown in Figure 1.

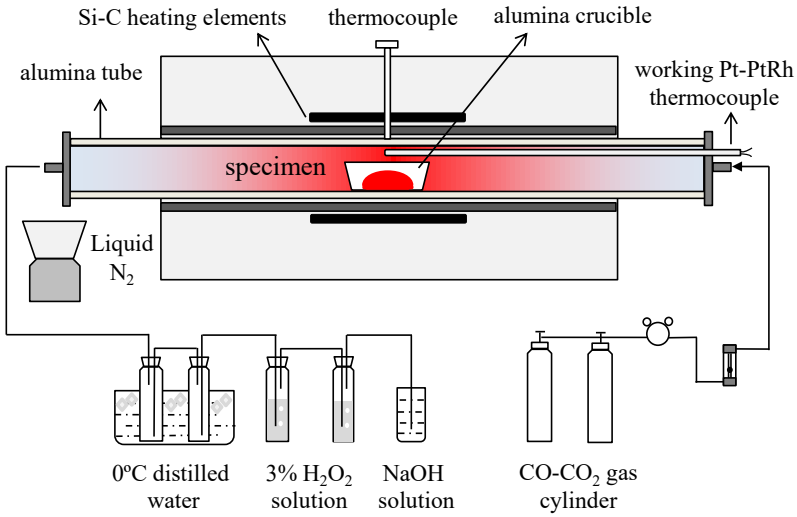

Figure 1. Schematic diagram of the experimental apparatus.

Alumina crucible was used to carry the specimen. 5 g $PbSO_4$ powder was evenly spread in alumina crucible and then loaded into the hot zone of the furnace. A Pt-PtRh working thermocouple was positioned immediately next to the specimen to measure the sample temperature. The furnace temperature was preset and heated up to the required level and held for fixed time. The left and right ends of the working tube were connected with CO-CO_2 inlet and off gas collection devices, respectively, and the gas was led into the working tube from the right. The reduction off-gas was discharged from the left and was collected and cleaned in four stages. The first two empty bottles submerged in distilled ice water (0 °C) were used to separate and collect the potential SO_3 gas (boiling point 16.8 °C) by condensation, while the SO_2 gas passed through and was collected in the following two 100 mL 3 % H_2O_2 wash bottles. The tail gas was absorbed by a NaOH solution. After experiments, the first two bottles were washed by 100 mL distilled water to dissolve and collect the captured SO_3.

The gas collection samples are analyzed by Inductively Coupled Plasma-Atomic Emission Spectrometry (ICP-AES, Perkin Elmer, Optima 3000, USA) to determine the total concentration of the collected SO_2 and SO_3 as H_2SO_4, then translate it to molar quantity of SO_2 and SO_3, respectively. The solid reduction samples were quenched in liquid N_2 after each test. X-ray Diffraction (XRD, D/max 2550PC, Rigaku Co. Ltd., Japan) and Scanning Electron Microscope and Energy Dispersive Spectroscopy (SEM-EDS, Carl Zeiss LEO 1450, Germany; EDS, INCA Wave 8570, Oxford Instruments, UK) were employed to determine the phase compositions and microstructures of the solidified reduction products.

$PbSO_4$ reduction degree γ was calculated according to following equation:

$$\gamma = \frac{M_{PbSO_4}\ \text{after decomposition}}{M_{PbSO_4}\ \text{before decomposition}} \times 100\ \% \tag{1}$$

Partial pressure of gas products SO_3 and SO_2 is determined by the ideal gas law $PV=nRT$, as:

$$p = \frac{n_{gas\ product} \times RT}{V} = \frac{8.314 \times n_{gas\ product} \times T}{t \times f} \tag{2}$$

where M: mass of $PbSO_4$, g; P: partial pressure of SO_3 or SO_2 gas, atm; V: total volume of gas, liters; n: SO_3 or SO_2 in moles; R: gas constant 8.314, $L \cdot atm \cdot mol^{-1} \cdot K^{-1}$; T: temperature, K; t: $PbSO_4$ reduction time, min; f: CO-CO_2 gas flow, L/min.

THERMODYNAMIC MODELLING

Figure 2 compared the gas-liquid-solid phases equilibrium compositions of $PbSO_4$ in the Ar and CO-CO_2 atmosphere. Figure 3 presents the PbO-$PbSO_4$ binary phase diagram. The figures were calculated by MTDATA ver. 8.2 software and its MTOX database. In the $PbSO_4$-Ar system, as shown in Figures 2 a, c and e, $PbSO_4$ self-decomposed gradually when temperature exceeded around 800 °C, and, as temperature increased, $PbSO_4$ decomposed to gas and a limited amount of PbO·$PbSO_4$. At the same time, PbO·$PbSO_4$ further melted and generated PbO(l) and $PbSO_4$(l) at around 972 °C. The amount of liquid oxide increased from 972 °C to around 1050 °C, and then decreased sharply, whereas, $PbSO_4$(l) continuously decomposed to PbO(l) and SO_2(g), O_2(g) and a small amount of SO_3(g). SO_3(g) further decomposed to SO_2(g) and O_2(g) as temperature increased. The total amount of gas continually rose up. Figure 2 (e) shows the gas species compositions, it is comprised of SO_2(g), O_2(g), PbO(g), Pb(g) and a limited amount of SO_3(g). Pb(g) generated from PbO(l) when temperature exceeded 1400 °C. Figure 3 illustrates that $PbSO_4$ and PbO·$PbSO_4$ mixture melts at 955 °C, $PbSO_4$ melts at around 1170 °C, and PbO melts at 886 °C. Therefore, in Ar, the decomposition mechanism of $PbSO_4$ is thermodynamically determined as that part of $PbSO_4$ firstly decomposes to PbO·$PbSO_4$ and emits SO_2(g) and O_2(g), then liquid PbO(l) and $PbSO_4$(l) starts to generate at 955 °C until $PbSO_4$ and PbO·$PbSO_4$ disappear in 972~1050 °C temperature range; Next, the liquid continuously decomposes, producing SO_3(g) (T>1000 °C), PbO(g) (T>1200 °C), and further releasing Pb(g) (T>1400 °C) together with SO_2(g) and O_2(g).

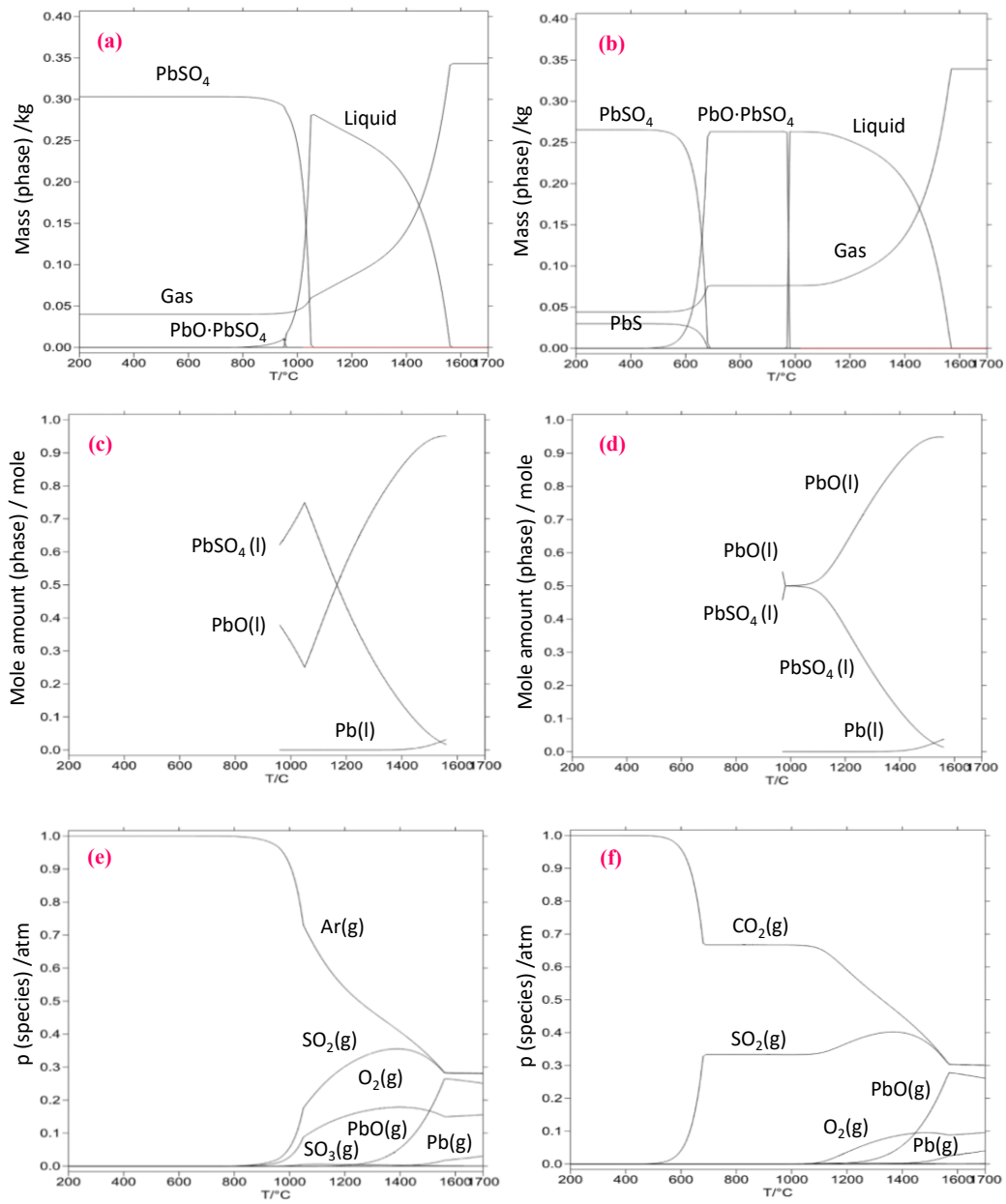

Figure 2. $PbSO_4$ equilibrium compositions in (a), (c), (e) Ar ($PbSO_4$: Ar = 1 : 1 mol) and (b), (d), (f) CO-CO_2 ($PbSO_4$: CO : CO_2 = 1 : 0.5 : 0.5 mol) system, the data were taken from MTDATA ver. 8.2 software and its MTOX database.

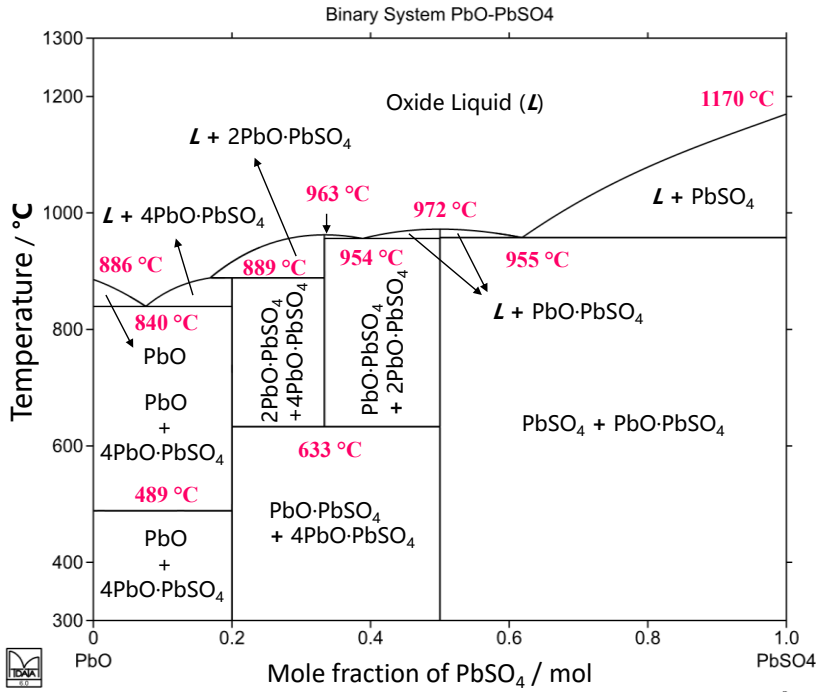

Figure 3. PbO-$PbSO_4$ binary phase diagram calculated using MTDATA ver. 8.2 software and its MTOX database.

However, in the $PbSO_4$-CO-CO_2 (1: 0.5 : 0.5 mol) system illustrated in Figures 2 (b), (d) and (f) , a part of $PbSO_4$ will firstly be reduced to PbS below 500 °C. The remaining $PbSO_4$ was decomposed to PbO·$PbSO_4$ and SO_2(g) in a temperature range around 500~700 °C. At the same time, PbS will also react with $PbSO_4$ to form PbO·$PbSO_4$ and SO_2(g) according to the reaction PbS+7$PbSO_4$=4(PbO·$PbSO_4$)+4SO_2 until PbS and $PbSO_4$ gradually disappeared. In the vicinity of 972 °C, PbO·$PbSO_4$ melted forming PbO(l) and $PbSO_4$(l). When temperature exceeded around 1050 °C, the liquid further decomposed, but no SO_3(g) formed. As temperature exceeded 1200 °C and 1400 °C, PbO(g) and Pb(g) were emitted, respectively. Therefore, in the reductive atmosphere, both reduction and self-decomposition of $PbSO_4$ occurred.

EXPERIMENTAL RESULTS AND DISCUSSION

$PbSO_4$ reduction thermogravimetric analysis

The TG-DTG-DSC curves of different mole ratios of $PbSO_4$-C mixture are presented in Figure 4. Figure 4 (a) shows that weight loss of $PbSO_4$-C mixture occurred above 436 °C, and two obvious weight loss zones, 13.96% and 10.46%, respectively, were detected. They ascribed to carbon gasification (seen from Figure 4 (b)) and $PbSO_4$ decomposition and reduction. At the same time, the DTA curves recorded two endothermic peaks, detected at 735.6 °C and 866.6 °C. They were associated to xPbO·$PbSO_4$ and PbS generation reactions. TG curves in Figure 4 (c) illustrates that an increasing carbon addition in the $PbSO_4$-C mixture caused a larger weight loss after deduction of the additional carbon.

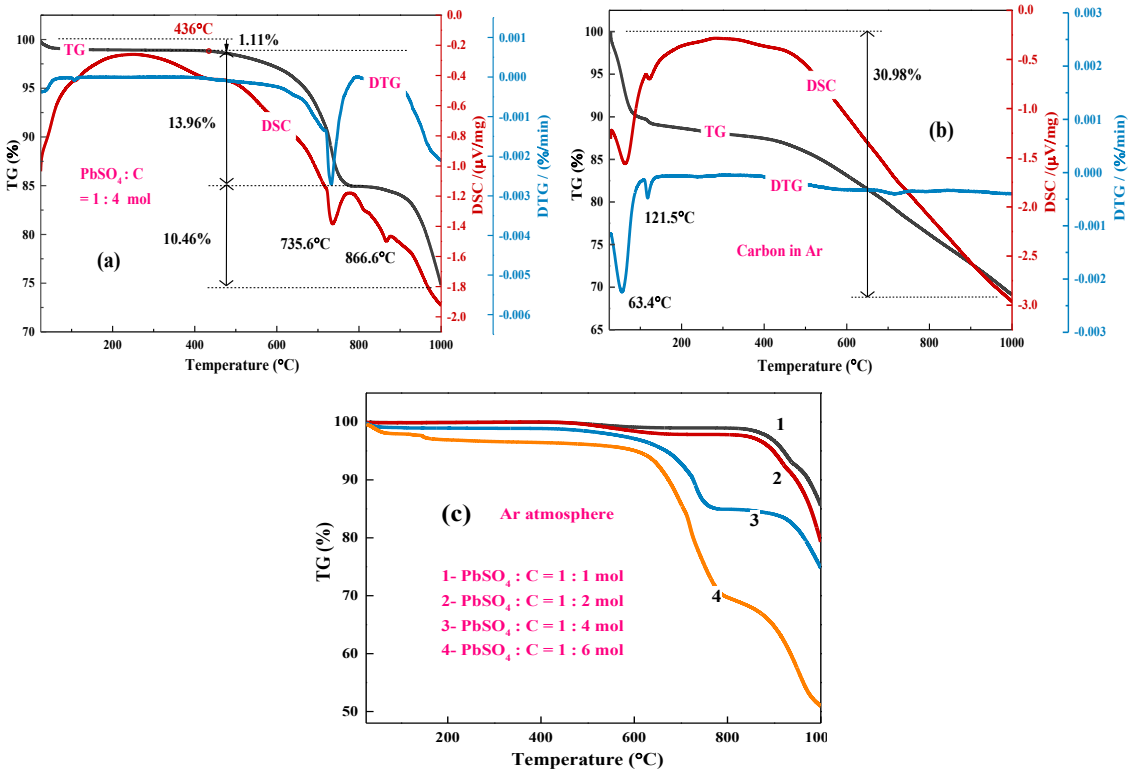

Figure 4. TG-DTG-DSC curves of (a) $PbSO_4$: C = 1:4 mixture; (b) carbon and (c) different mole ratio of $PbSO_4$-C mixture in Ar atmosphere (heating rate 10 °C/min, Ar gas flow 0.1 NL/min, NL is normal litre at 1 atm and 25 °C)

$PbSO_4$ reduction experimental phase conversion mechanisms

The XRD patterns of $PbSO_4$ reduction products at different CO-CO_2 atmospheres, variable temperatures and reduction times are presented in Figure 5. The results in Figures 5 (a)-(b) show that at a relatively low CO concentration 5% and 10% CO, PbO·$PbSO_4$ appeared at 700 °C before 2 h reaction. With temperature further increased, 2PbO·$PbSO_4$, PbS, 4PbO·$PbSO_4$ and individual PbO were generated successively. Furthermore, at the same temperature 867 °C and same reduction time 2 h, metallic Pb appeared in the 10% CO reduction system while the major phase formed in 5% CO system was 4PbO·$PbSO_4$. This suggests that a strongly reductive atmosphere can promote the $PbSO_4$ reduction.

Figures 5(c)-(f) illustrate that at a relatively high CO concentration 15% and 20% CO system, $PbSO_4$ was reduced to PbO·$PbSO_4$ below 600 °C in less than 1 h reduction time. At 700 °C, PbS was reduced from $PbSO_4$ after 1 h reaction in the 15% CO atmosphere. When temperature rose up to 800 °C, in 15% CO reduction system, the main products after 1 h and 2 h were PbO·$PbSO_4$ and 2PbO·$PbSO_4$, respectively, as Figures 5(c) and (e) show. However, in the 20% CO reduction system, PbS dominated the reduction product within 1 h reaction time. No obvious PbS diffraction peaks were detected until 867 °C and 2 h reduction time in the 15% CO system, as shown in Figure 5(f). This indicates that a suitable reductive atmosphere and temperature can change $PbSO_4$ reduction mechanisms and path from $PbSO_4$→PbO·$PbSO_4$→2PbO·$PbSO_4$→4PbO·$PbSO_4$→PbO→Pb to $PbSO_4$ →PbS.

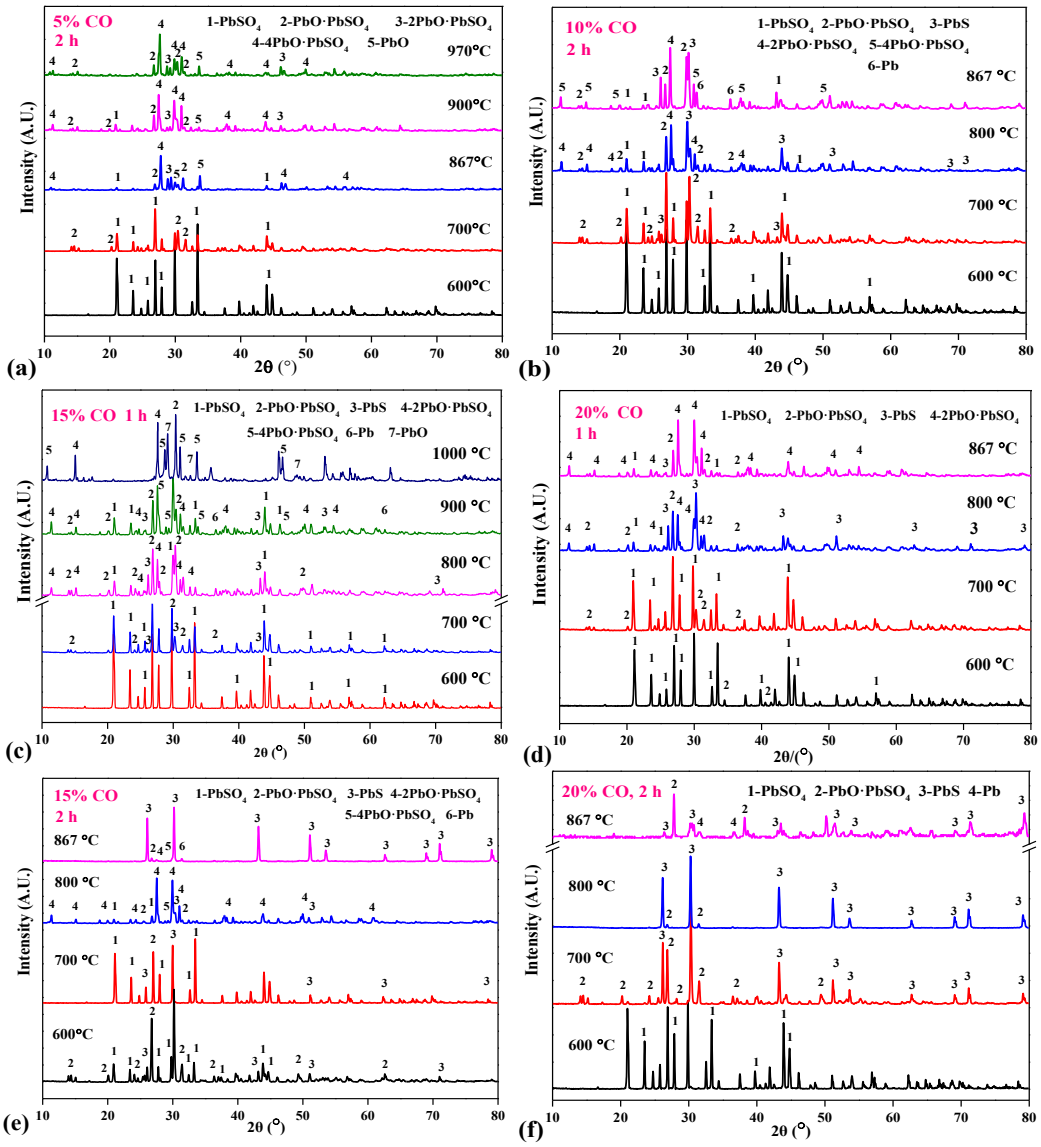

Figure 5. XRD patterns of $PbSO_4$ reduction products at different temperatures, times and variable reductive atmospheres; (a) reduction in the 5% CO for 2 h, (b) reduction in the 10% CO for 2 h, (c) reduction in the 15% CO for 1 h, (d) reduction in the 20% CO for 1 h, (e) reduction in the 15% CO for 2 h and (f) reduction in the 20% CO for 2 h (CO-CO_2 gas flow 0.1 NL/min).

Figure 6 presents SEM-EDS results of the solid reduction products generated in different reduction systems. Figures 6 (a)-(f) show that $PbO·PbSO_4$ was preferentially reduced from $PbSO_4$ particles and changed to an irregular loose substance and filled the interspaces of $PbSO_4$ particles. Then $PbO·PbSO_4$ was further reduced and gathered to dense cake of $2PbO·PbSO_4$, $4PbO·PbSO_4$ and PbO. PbS would be reduced directly and *in situ* from $PbSO_4$ particles in high CO systems in Figures 6 (g)-(i). A small amount of $PbSO_4$ was also reduced through the $PbSO_4 \rightarrow 2PbO·PbSO_4 \rightarrow PbO$ path. Thus, PbS, PbO and $2PbO·PbSO_4$ coexisted during the reduction, but PbS dominated in the end product.

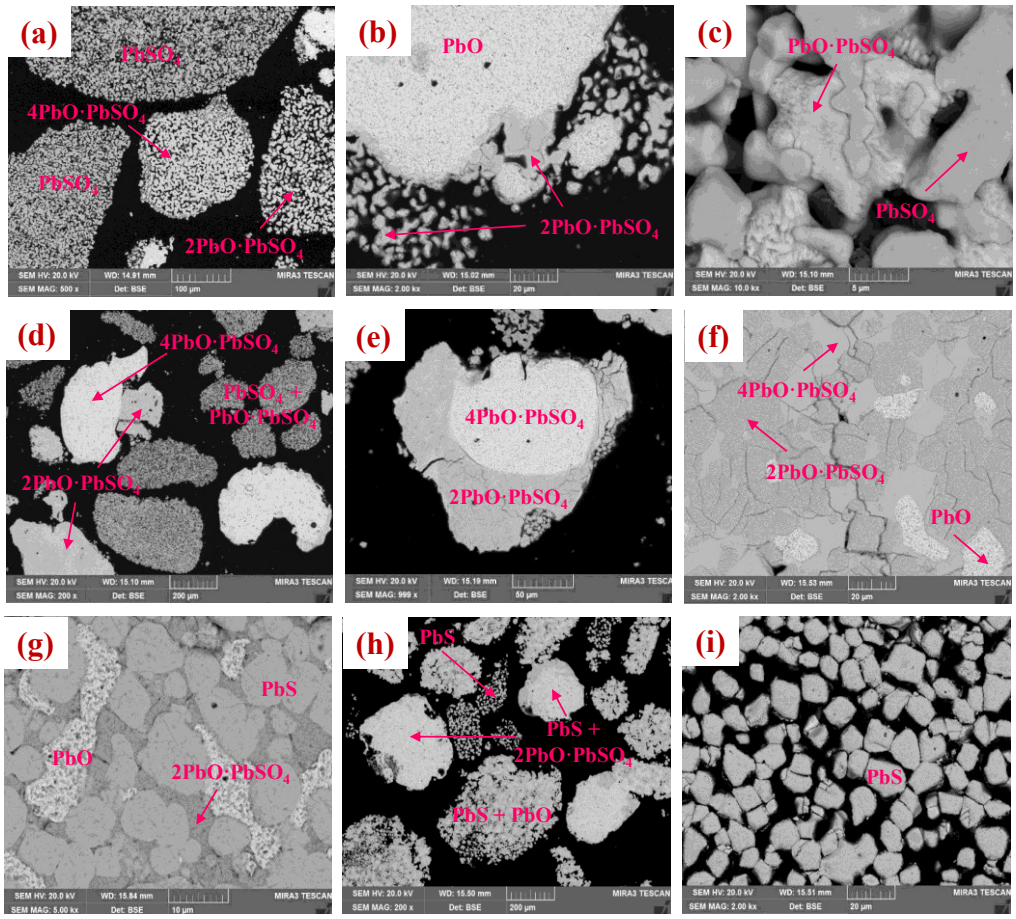

Figure 6. SEM micrographs of $PbSO_4$ reduction products at different temperatures, times and atmospheres: **(a)-(b)** 5% CO, 867 °C, 2 h; **(c)-(e)** 10% CO, 900°C, 1 h; **(f)** 15% CO, 900 °C, 1 h; **(g)** 15% CO, 800°C, 2 h; **(h)-(i)** 20% CO, 800°C, 2 h.

$PbSO_4$ reduction degree, gas compositions and its changing mechanisms

$PbSO_4$ reduction degree vs. CO% concentration, temperature and reduction time curves are shown in Figures 7 (a)-(b). The results indicate that $PbSO_4$ reduction degree increased along with temperature, CO% concentration and time. This is in full agreement with the above results by thermogravimetric analysis. Figures 7 (c)-(f) illustrate SO_2 and SO_3 partial pressures (p_{SO_2} and p_{SO_3}) in the $PbSO_4$ reduction process off-gas in the isothermal experiments. It shows that the SO_2 and SO_3 gas species were indeed generated during the experimental $PbSO_4$ reduction at laboratory scale.

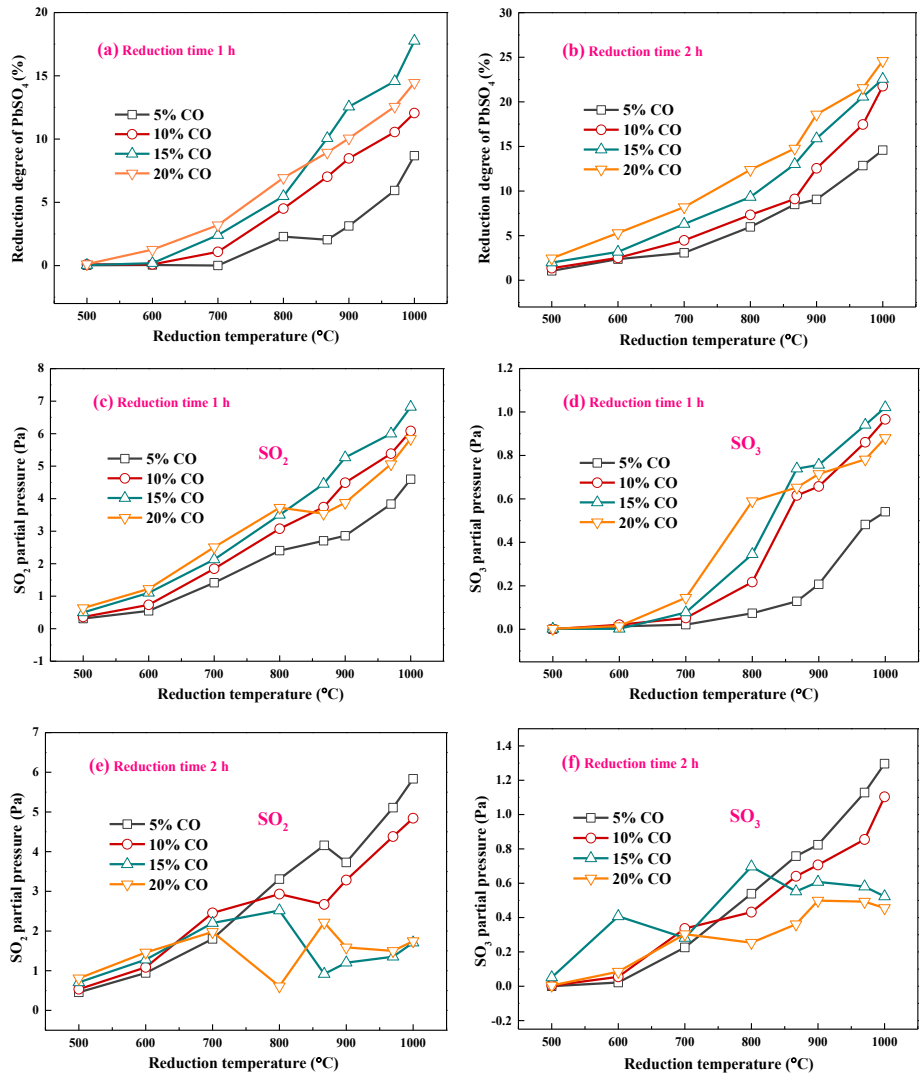

Figure 7. Effect of different atmospheres, temperature and the reaction time on (a)-(b) $PbSO_4$ reduction degree, (c)-(f) p_{SO_2} and p_{SO_3} in $PbSO_4$ reduction off-gas (CO-CO_2 gas flow 0.1 NL/min)

It can be observed in Figures 7 (c)-(d) that, p_{SO_2} and p_{SO_3} increased along with increasing of temperature and CO concentration in the process gas. Additionally, p_{SO_2} was greater than p_{SO_3} and SO_2 was the major sulfur-bearing off-gas species in the outlet because $SO_{3(g)}$ tended to decomposed to $SO_{2(g)}$ and $O_{2(g)}$ at high temperatures. This is in full agreement with the thermodynamic calculations. However, considering Figure 2(d), SO_3 should not generate in the reductive environments. Therefore, the observed SO_3 existence indicates that direct $PbSO_4$ decomposition reactions also took place in the reduction system but at a very slow rate:

$$PbSO_4 = 1/2\ (PbO{\cdot}PbSO_4) + 1/2\ SO_{3(g)} \qquad \Delta G_T^\theta = -0.0197T + 22.67,\ 0\ °C < T < 1000\ °C \tag{3}$$

$$(PbO{\cdot}PbSO_4) = 2/3\ (2PbO{\cdot}PbSO_4) + 1/3\ SO_{3(g)} \qquad \Delta G_T^\theta = -0.050\ T + 80.852,\ 0\ °C < T < 1000\ °C \tag{4}$$

$$(2PbO{\cdot}PbSO_4) = 3/5(4PbO{\cdot}PbSO_4) + 2/5\ SO_{3(g)} \qquad \Delta G_T^\theta = -0.067\ T + 116.25 \tag{5}$$

$$(4PbO{\cdot}PbSO_4) = 5\ PbO + SO_{3(g)} \qquad \Delta G_T^\theta = -0.0197\ T + 35.07,\ 0\ °C < T < 1000\ °C \tag{6}$$

$$(2PbO{\cdot}PbSO_4) = 3\ PbO + SO_{3(g)} \qquad \Delta G_T^\theta = -0.186\ T + 301.85 \tag{7}$$

$$(PbO{\cdot}PbSO_4) = 2\ PbO + SO_{3(g)} \qquad \Delta G_T^\theta = -0.168\ T + 279.17 \tag{8}$$

$PbSO_4 = PbO + SO_{3(g)}$ $\Delta G_T^\theta = -0.151\ T + 246.37$ (9)

$2\ SO_{3(g)} = 2\ SO_{2(g)} + O_{2(g)}$ $\Delta G_T^\theta = -0.045\ T + 34.959$ (10)

The Gibbs energies ΔG_T^θ of the reactions above were calculated by HSC 9.2.6 software and its database [29] (unit of ΔG_T^θ is *kJ/mol*, temperature T is *°C*).

In Figures 7 (e)-(f), with extending reduction time, partial pressures of SO_2 and SO_3 gradually decreased after 800 °C. This implied that the SO_2 and SO_3 generation reactions slowed down. Combined with the XRD patterns in Figures 5 (e)-(f), the $PbSO_4$ reduction and decomposition mechanism changed from 'decomposition dominated' $PbSO_4 \rightarrow PbO \cdot PbSO_4 + SO_2/SO_3 \rightarrow 2PbO \cdot PbSO_4 + SO_2/SO_3 \rightarrow 4PbO \cdot PbSO_4 + SO_2/SO_3 \rightarrow PbO + SO_2/SO_3 \rightarrow Pb$ to a 'reduction dominated' $PbSO_4 \rightarrow PbS$ sequence. Sulfur-containing gas SO_2 and SO_3 generation was limited, and sulfur was fixed in the system as PbS. This suggests that $PbSO_4 \rightarrow xPbO \cdot PbSO_4 + SO_2/SO_3$ reactions mainly occurred at low CO concentrations and in a low temperature range. In a proper strongly reductive atmosphere and at high-enough temperature, $PbSO_4$ will be selectively reduced to PbS. Thus, sulfur present in the feed as $PbSO_4$ will remain as PbS in the product without generating gaseous SO_2 and/or SO_3. However, the reduction temperature cannot be too high, because the high vapor pressures of the reduced by-products PbS and PbO will cause dust losses of lead in the off-gas. Possible $PbSO_4$ reduction mechanisms are graphically summarized as Figure 8.

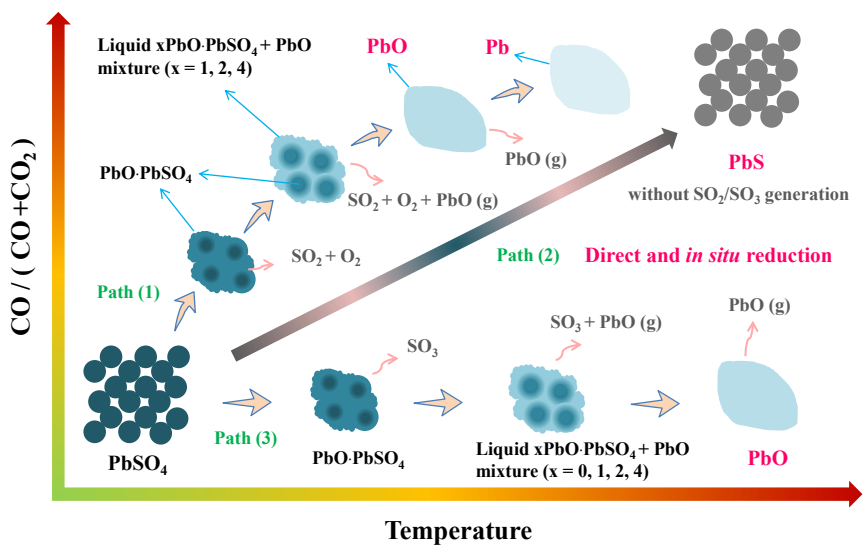

Figure 8. Schematic of $PbSO_4$ reduction phase conversions and microscopic transformation mechanisms

CONCLUSION

Lead-containing wastes can be recycled using a novel, promising reductive sulfur-fixing co-smelting technique to recover various valuable components and immobilize sulfur as condensed sulfide matte. Thus, the low-concentration sulfur-containing off-gas generation and its environmental pollution are expected to be reduced significantly and can be captured e.g. by scrubbing.

This paper investigated reduction mechanisms of the major component, $PbSO_4$, in lead-bearing wastes during the RSFCS process. Thermodynamic modelling, thermogravimetric, XRD and SEM-EDS analysis showed that three different transformation paths exist in the $PbSO_4$ reduction process:

(1) $PbSO_4 \xrightarrow{CO/CO_2} PbO \cdot PbSO_4 + SO_2 \xrightarrow{CO/CO_2} 2PbO \cdot PbSO_4 + SO_2 \xrightarrow{CO/CO_2} 4PbO \cdot PbSO_4 + SO_2 \xrightarrow{CO/CO_2} PbO + SO_2 \xrightarrow{CO/CO_2} Pb$;

(2) $PbSO_4 \xrightarrow{CO/CO_2} PbS$;

(3) $PbSO_4 \rightarrow PbO \cdot PbSO_4 + SO_3 \rightarrow 2PbO \cdot PbSO_4 + SO_3 \rightarrow 4PbO \cdot PbSO_4 + SO_3 \rightarrow PbO + SO_3$.

Through paths (1) and (3), $PbSO_4$ was reduced to PbO, Pb and SO_2/SO_3 gas, while the reduction path (2) allowed PbS formation without generation of gaseous SO_2/SO_3 in the process off-gas.

Reduction temperature and the CO concentration in the gas feed showed the major effects on the $PbSO_4$ reduction path and degree of reduction. In a relatively weakly reductive atmosphere (generally CO less than

10 vol%) and low temperature range (below around 700 °C), the reduction paths (1) and (3) dominated, but path (1) was the main reduction route.

Thus, $xPbO \cdot PbSO_4$ (x=1, 2, 4), PbO and SO_2 were the major products at low temperatures. When temperature and reductivity of the process gas increased, the direct $PbSO_4$ reduction was emphasized, and the reduction path $PbSO_4 \xrightarrow{CO/CO_2} PbS$ was increasingly dominated. The experimental results suggested that controlling the process temperature at 800~900°C, using CO concentrations within 15-20 vol% and a flow rate of 0.1 NL/min, 5 g $PbSO_4$ can be selectively reduced to PbS within a 2 h reaction time, and the sulfur in $PbSO_4$ fixed in the condensed product as PbS, instead of emitting to off-gas as gaseous SO_2 and SO_3.

ACKNOWLEDGEMENTS

This work is supported by China Postdoctoral Science Foundation (Grant No. BX20200391); Hunan Provincial Science Fund for Distinguished Young Scholars, China [Grant No. 2018JJ1044]; the Regional Program of the National Natural Science Foundation of China (Grant No. 51664013); Program for Young Talents of Science and Technology in Universities of Inner Mongolia Autonomous Region (Grant No. NJYT-17-B35) and Bayannur Science and Technology Project from Bayannur Bureau for Science and Technology (Grant No. K201509).
There is no conflict of interest.

REFERENCES

1. D. Gregurek, Z. Peng and C. Wenzl, *JOM*, 67, 1986 (2015).
2. X. Zhang, L. Li, E. Fan, Q. Xue, Y. Bian, F. Wu and R. Chen, *Chem. Soc. Rev.*, 47, 7239 (2018).
3. P. Frohlich, T. Lorenz, G. Martin, B. Brett and M. Bertau, *Angew. Chem. Int. Ed. Eng.*, 56, 2544 (2017).
4. C. S. Brooks, *Metal recovery from industrial waste*, CRC Press, 2018.
5. Y. Li, S. Yang, W. Lin, P. Taskinen, J. He, Y. Wang, J. Shi, Y. Chen, C. Tang and A. Jokilaakso, *Minerals*, 9, 119 (2019).
6. L. Zhang, *Morden lead metallurgy*, Central South University Press, Changsha, China, 2013.
7. X. Tian, Y. Wu, S. Qu, S. Liang, W. Chen, M. Xu and T. Zuo, *J. Clean. Prod.*, 199, 391 (2018).
8. B. Blanpain, S. Arnout, M. Chintinne and D. R. Swinbourne, "*Lead Recycling*", in *Handbook of Recycling*, Elsevier, 2014.
9. X. Tian, Y. Wu, P. Hou, S. Liang, S. Qu, M. Xu and T. Zuo, *J. Clean. Prod.*, 144, 142 (2017).
10. A. Pinasseau, B. Zerger, J. Roth, M. Canova and S. Roudier, *Eur. Comm. Ind. Emiss. Dir.*, 75, (2010).
11. C. O. Onwosi, V. C. Igbokwe, J. N. Odimba, I. E. Eke, M. O. Nwankwoala, I. N. Iroh and L. I. Ezeogu, *J. Environ. Manage.*, 190, 140 (2017).
12. W. Zhang, J. Yang, X. Wu, Y. Hu, W. Yu, J. Wang, J. Dong, M. Li, S. Liang and J. Hu, *Renew. & Sustain.Ener. Rev.*, 61, 108 (2016).
13. X. Ma, S. Wang and X. Li, *Mater. Res. Appl*., 2, 141 (2008).
14. D. Andrews, A. Raychaudhuri and C. Frias, *J. Power Sources*, 88, 124 (2000).
15. Y. Li, S. Yang, P. Taskinen, J. He, Y. Chen, C. Tang, Y. Wang and A. Jokilaakso, *JOM*, 71, 1 (2019).
16. Y. Zheng, W. Liu, W. Qin, F. Jiao, J. Han, K. Yang and H.. Luo, *J Cen. South Univ.*, 22, 2929 (2015).
17. Y. Li, C. Tang, Y. Chen, S. Yang, L. Guo, J. He and M. Tang, *8th International Symposium on High-Temperature Metallurgical Processing,* Springer, 767 (2017).
18. L. Ji. and S. Jin, *Sulphuric Acid Ind.*, 04, 1 (2016).
19. C. Mohanty, S. Adapala and B. Meikap, *J. Hazard. Mater.*, 165, 427 (2009).
20. Y. Li, S. Yang, P. Taskinen, J. He, F. Liao, R. Zhu, Y. Chen, C. Tang, Y. Wang and A. Jokilaakso, *J. Clean. Prod.*, 217, 162 (2019).
21. Y. Li, Doctoral Thesis, Aalto University, 2019. DOI: https://aaltodoc.aalto.fi/handle/123456789/38022.
22. Y. Li, Y. Chen, C. Tang, S. Yang, L. Klemettinen, M. Rämä, X. Wan and A. Jokilaakso, in *Extraction 2018*, Springer, 1109 (2018).
23. Y. Li, S. Yang, P. Taskinen, J. He, Y. Chen, C. Tang and A. Jokilaakso, *JOM*, 72, 7 (2019).
24. Y. Li, S. Yang, P. Taskinen, Y. Chen, C. Tang and A. Jokilaakso, *Metals*, 9, 911 (2019).
25. Q. Liu, J. Tan, C. Q. Liu, Z. L. Yin, Q. Y. Chen, L. Zhou, F. C. Xie and P. M. Zhang, *Chin. J. Nonferr. Metals*, 24, 1629 (2014).
26. M. Scheidema, Doctoral Thesis, Aalto University, 2015. DOI: https://aaltodoc.aalto.fi/handle/123456789/17902.
27. R. Davies, A. Dinsdale, J. Gisby, J. Robinson and S. Martin, *CALPHAD Comput. Coupling Phase Diagr. Thermochem*., 26, 2, 229 (2002).
28. J. Gisby, P. Taskinen, J. Pihlasalo, Z. Li, M. Tyrer, J. Pearce, K. Avarmaa, P. Björklund, H. Davies, M. Korpi, S. Martin, L. Pesonen and J. Robinson, Metall. & Mater. Trans. B, 48B, 91 (2017).
29. A. Roine, HSC Chemistry. *Outokumpu Research Oy,* Pori, Finland, 2019, DOI: www.hsc-chemistry.com.